ELSEVIER

Journal of Biomechanics 37 (2004) 1001–1009

JOURNAL OF BIOMECHANICS

www.elsevier.com/locate/jbiomech
www.JBiomech.com

Load transfer across the scapula during humeral abduction

Sanjay Gupta[a,b,*], Frans C.T. van der Helm[a]

[a] Department of Mechanical Engineering and Marine Technology, Faculty of Design, Engineering and Production, Man-Machine Systems Group, Delft University of Technology, Mekelweg 2, 2628 CD Delft. The Netherlands

[b] Department of Applied Mechanics, Bengal Engineering College (Deemed University), Howrah, West Bengal 711103, India

Accepted 19 November 2003

Abstract

1. Introduction

The shoulder mechanism is an example of a very complex musculoskeletal structure, and consists of a chain of bones connecting the humerus to the trunk. The shoulder consists of scapula and clavicle and functions as a movable but stable base for the motions of the humerus. The scapula is connected to the clavicle by the acromioclavicular (AC-) joint and to the thorax by the scapulothoracic gliding plane (STGP). The sterno-clavicular (SC-) joint connects the clavicle to the sternum. The humerus articulates with the scapula at the glenohumeral (GH-), representing a ball-and-socket joint.

The scapula is subject to a number of muscle, ligament and joint reaction forces during elevation of the arm. Quantitative and qualitative estimates of all the muscles, ligaments and joint reaction forces acting on the scapula, during humeral abduction have been obtained (Van der Helm, 1994a,b). It seems from the location, magnitude and direction of these forces that the scapula is loaded all over its structure. The primary function of the scapula is two-fold. On the one hand it offers an additional joint, so that the total rotation of the humerus with respect to the thorax can increase. On the other, it is a large bone, where the muscles have large lever arms with regard to the SC- and the AC-joint. Hence, smaller muscles will be sufficient to provide the necessary moments, which are in general larger than the moments around the GH-joint. The shape of the scapula provides large moments about the SC- and the AC-joint. This function is more important for the particular shape of the scapula.

The load transfer and stress distribution across the scapula has not been discussed until now. Studies that were mostly restricted to 2D and 3D models of the

*Corresponding author. Department of Applied Mechanics, Bengal Engineering College (Deemed University), Howrah, West Bengal 711103, India. Tel.: +91-33-2668-4561; fax: +91-33-2668-4564.
E-mail address: sgupta@appmech.becs.ac.in (S. Gupta).

0021-9290/$ - see front matter
doi:10.1016/j.jbiomech.2003.11.025

implanted glenoid were unable to describe it (Orr et al., 1988; Friedman et al., 1992; Lacroix et al., 1997; Stone et al., 1999; Lacroix et al., 2000; Couteau et al., 2001). These models lack the ability to describe the complex geometry and loading adequately, since other important bony structures (e.g. scapula spine, medial border, lateral border, infraspinous and supraspinous fossa), joints (e.g. AC, STGP) and the effect of muscles, ligaments, and joint reaction forces were omitted. Stress analysis of the natural scapula is required to understand how the loading is being transferred to various parts of the scapula and to compare the deviations in stress patterns due to glenoid arthroplasty. The 3D model of Lacroix et al. (1997) and Lacroix et al. (2000), using computed tomography (CT) scan data, was an effort in this direction. However, the quality of mesh generation (total elements: 7251 total degrees of freedom: 29415) is considered to be coarse. Moreover, neither a validation nor the errors in the FE model was discussed (Lacroix et al., 1997, 2000), which makes it difficult to assess the accuracy of the results. The model might be able to predict certain qualitative trends, but lacks the ability to understand, in detail, the stresses generated in various parts of the scapula due to the action of muscles, ligaments and joint reaction forces, quantitatively.

The scapula is a large, flat, triangular bone with a very complex structure. There are five thick bony ridges (glenoid, scapular spine, medial and lateral border, and coracoid process) and two thin, hard laminated structures—the infraspinous and supraspinous fossa. The glenoid is the lateral angle of the triangular flat bone and the scapular spine originates from the flat bone plate, the infraspinous fossa. The infraspinous fossa is surrounded by the lateral and medial border. A computationally efficient and accurate 3D FE model of a natural scapula is required to study the load transfer mechanism. A novel technique, combining shell and solid elements, was used to develop a FE model of the scapula that was experimentally validated using strain gage measurements (Gupta et al., in press). Using this 3D FE model and the musculoskeletal shoulder model of forces (Van der Helm, 1994a,b), the purpose of this study was to evaluate stress distributions in the constituent structures of the scapula, during elevation of the arm. The study also aims at understanding the function of coracoacromial ligament, which from anatomical point-of-view appears to be a tensional brace protecting the acromion in abduction and retroversion of the humerus.

2. Materials and methods

A 3D FE model of the natural scapula was developed, using CT data and shell-solid modelling approach. Ten-node tetrahedral solid elements were used to model cancellous bone and a part of the compact bone layer of the thick bony structures of the scapula, whereas eight-node quadrilateral shell elements were used to represent the infraspinous and supraspinous fossa. The outer cortical bone was modelled using two-layered triangular shell elements, with 0.5 mm thickness of each layer. The material properties all elements and thickness of shell elements were based on CT-scan data. The range of elastic modulus of cancellous bone varied from 1 to 128 MPa for open cell structure, and from 128 to 17500 MPa for closed cell structure. The edge lengths of elements were specified between 2–4 mm or smaller on a side, and mesh generation was obtained using ANSYS FE software. The FE model, as shown in Fig. 1, contained 10921 elements (tetrahedrals: 7412, quadrilateral shells: 357, triangular layered shells: 357), 14086 nodes, and a total number of 63435 active DOF. The model was solved using ANSYS software.

The accuracy of the results was checked, using some comparison and a convergence study based on stresses in the areas of interest was required. The first coarse model consisted of 6253 elements, 8000 nodes and a total number of 37164 DOF. The second case corresponds to the present FE model, after mesh refinement. In the present problem (a blend of 3D and 2D elements), a uniform mesh refinement with factor 2 would lead to 4–8 times DOF. The solution of such large size FE model was hindered by required computer resources and software limitations. Hence, local mesh refinement was judiciously performed on areas with high stress gradient. In the third case, mesh refinement with element size less than 3 mm, was performed in the thick bony regions, resulting in 14,582 elements, 18,720 nodes and a total number of 82701 DOF. Comparison of results between the first and the second case indicated differences of stresses (principal normal and Von Mises) in the order of 11–13%. Whereas, these deviations were significantly reduced (0.6–1%), when the results were compared between the second (present) and the third model. Therefore, the present mesh would be sufficient to calculate stress distribution in the scapula.

2.1. Coracoacromial ligament

The coracoacromial ligament is connected between the anterior side of acromion and the cranial side of coracoid process (Levy and Copeland, 2001). The qualitative and quantitative functions of this ligament are unknown. In order to assess the qualitative function of this ligament in the scapula, two additional beam elements were introduced in the FE model (Fig. 2). Nodes located on the anterior side of acromion and coracoid process were connected to create these beam elements. Since reliable data on the geometry and the material properties of this ligament were unknown, the role of this ligamentous structure, which insert on

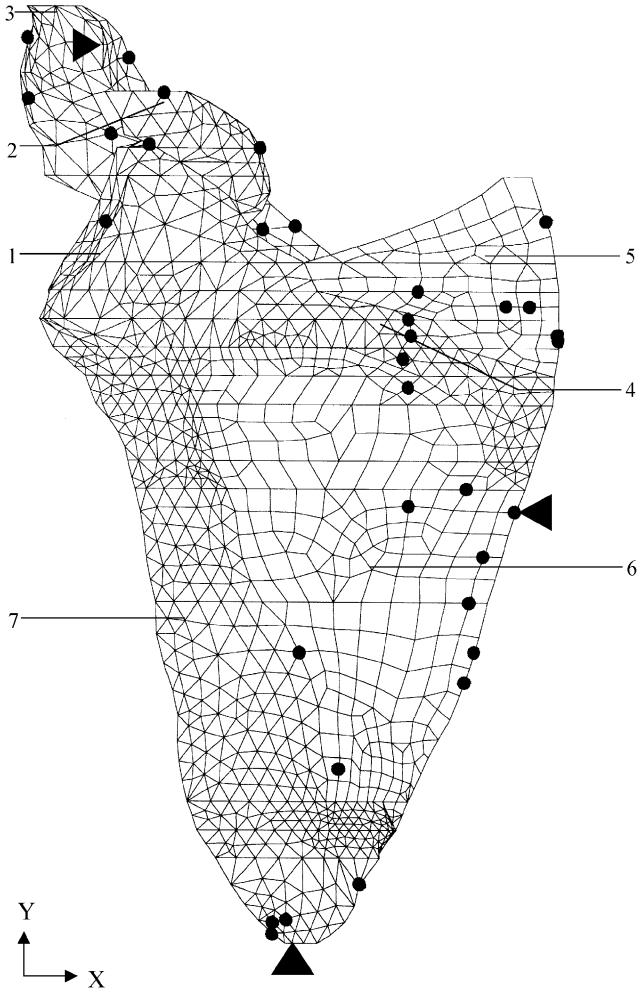

Fig. 1. Finite element model of the scapula: (1) glenoid; (2) coracoid process; (3) acromion; (4) scapular spine; (5). supraspinous fossa; (6) infraspinous fossa; (7) lateral border. • Point of application of force; ▲ node restraint to translate in all directions ($U_x = U_y = U_z = 0$); ◀ node restraint to translate in x- and z-directions ($U_x = U_z = 0$); ▶ node restraint to translate in z-direction ($U_z = 0$).

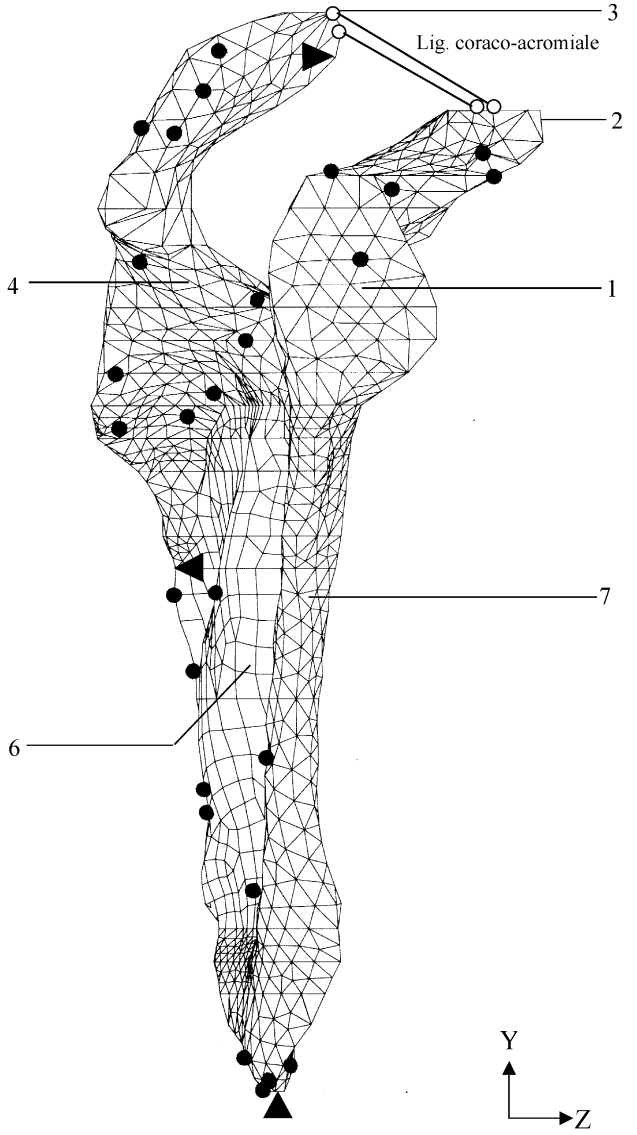

Fig. 2. A lateral view of FE model of the scapula showing the ligament coraco-acromiale as two beam elements formed by connecting nodes (o); for more explanations see Fig. 1.

different points of the same bone, on the stress distribution of the whole scapula could not be predicted in this study. Hence, a very low value of Young's modulus, 100 MPa and unit cross sectional area and thickness were assumed, so that only the lengthening and shortening of the ligament can be calculated without affecting the load distribution of the scapula.

2.2. Applied loading conditions

The musculoskeletal shoulder model (Van der Helm, 1994a,b) and the CT images were based on the same cadaver. Geometric transformations were calculated to relate the shoulder model to the CT image and finally to the FE model. Van der Helm and Veenbaas (1991) reported that generally more than one muscle lines of force were necessary to adequately represent the mechanical effect of muscles with large attachment sites. Each muscle was represented by one to six elements, where each element can be considered as a single independent muscle line of force (Van der Helm and Veenbaas, 1991). During humeral abduction, the muscle elements change their length as well as orientation with respect to each other. A total number of 95 muscle elements were used to define all the shoulder muscles in the model. A schematic diagram of the major muscle and joint reaction forces acting on the scapula is presented in Fig. 3. All muscle, ligament and joint reaction forces for six load cases (unloaded abduction from 30–180°), calculated from the shoulder model of forces (Van der Helm, 1994a,b), were used as applied loading conditions for the FE model (Fig. 1). The nearest node numbers on the surface of the FE model, corresponding to a point of force application, were

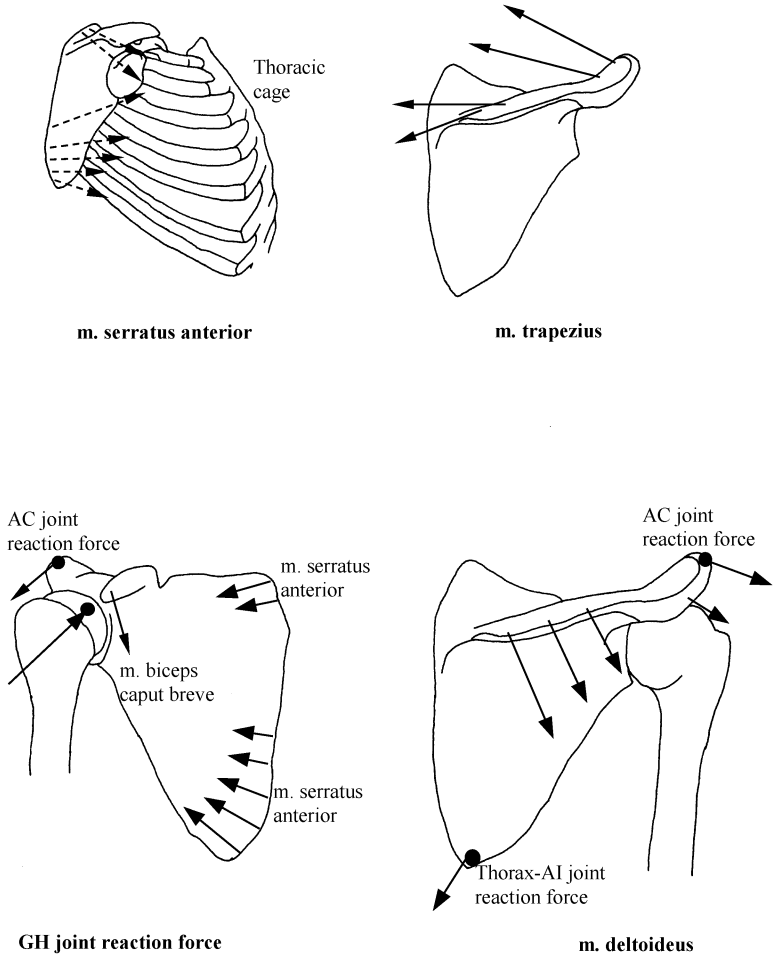

Fig. 3. Schematic diagram of the major muscle and joint reaction forces.

computed. All the forces were applied as concentrated forces on these node numbers, since data on area of the attachment sites of muscles and ligaments were not available.

The constraints in the FE analysis served to counteract residual moments (from errors in applying the forces) and to prevent rigid body motion. The procedure of locating the nearest node number in the FE model, corresponding to a point of application of force, resulted in a small shift of the point of application, introducing an error in the form of residual moments as compared to the state of moment equilibrium in the shoulder model (Van der Helm, 1994a,b). Prescription of physiological constraints was used to correct for residual moments that should be reasonably small. Some forces from this shoulder model (Van der Helm, 1994a,b) such as thorax-angulus inferior (thorax-AI) reaction force (F_x, F_y, F_z), AC-joint reaction (F_z) and a part of the m. serratus anterior (F_x, F_z), were replaced by constraints. The choice of replaced muscle by constraints was based on several iterative solutions. Constraints were so chosen that the difference (i.e. residual force) between the reactive force calculated by the FE model and the originally replaced force was minimal. Hence, the scapula was less artificially constrained. The location and type of constraints, applied at three nodes located farthest from each other, are shown in Figs. 1 and 2. The consequences of using these constraints were checked so that they had minimum effect on the stress distribution of the scapula.

The action of muscle, ligaments and joint reaction forces has considerable effect on the stresses evoked in the individual bony ridges, constituting the scapula. The force and moment analyses are presented with respect to a local co-ordinate system. The origin of the local co-ordinate system is at the thorax-trigonum spinae (thorax-TS) connection, with the x-axis along the scapular spine pointing from medial to lateral (TS-AC), the y-axis is in the scapular plane defined by AC-TS-AI, pointing from caudal to cranial and z-axis from ventral to dorsal. During 90° humeral abduction, the forces are higher as compared to other six load cases. Therefore, the results for this load case are chosen for more detailed interpretation.

Table 1
The reactive forces (Rf_x, Rf_y, Rf_z) in N, along x-, y- and z-axis, calculated by the FE model at the three constraints located at thorax-angulus inferior (thorax-AI), thorax-trigonum spinae (thorax-TS) and acromion, during 90° unloaded abduction located, as calculated by the FE model (Fig. 1)

Constraints (location)	Force (calculated) (Rf_x)	Force (omitted) (F_x)	Residual force ($Rf_x - F_x$)	Force (calculated) (Rf_y)	Force (omitted) (F_y)	Residual force ($Rf_y - F_y$)	Force (calculated) (Rf_z)	Force (omitted) (F_z)	Residual force ($Rf_z - F_z$)
Thorax-AI	−62.05	−53.69	8.36	1.11	1.11	0.0	−111.03	−102.48	8.55
Thorax-TS	10.71	2.35	8.36				12.14	3.36	8.78
Acromion							−66.37	−66.14	0.23
Total	−51.34	−51.34	0.0	1.11	1.11	0.0	−165.26	−165.26	0.0

These forces correspond to the forces that were left unspecified in the FE model and replaced by physiologic constraints.

3. Results

The reactive forces as calculated by the FE model during 90° abduction is presented in Table 1. The differences (residual forces) between these calculated forces and the original forces that were omitted varied between 0–8 N. The reactive forces induced at the constraints located at the thorax-AI and the acromion were well comparable to the originally omitted forces (0–15% change), except the constraint at the thorax-TS connection (Table 1). The effect on the stress distribution due to residual (additional) forces (Rf_x and Rf_z) of 8 Newton at this location was, however, quite localised.

The distributions of principal stresses (tensile and compressive) during 90° unloaded abduction are presented in Fig. 4. A quantitative and qualitative estimate of the load transfer mechanism on individual parts of the scapula is presented in the following sections.

3.1. Acromion

The moments around the AC-joint were side effects of the muscle activity needed around the SC- and GH-joint, since no monoarticular muscle is crossing the joint. The acromion is subject to the combined effect of the following forces, (1) the AC-joint reaction force due to the pressing of the scapula against the clavicle, (2) the m. trapezius, scapular part (3) the m. deltoideus, scapular part. The combined effect of the pulling force by m. deltoideus and m. trapezius, and the AC-joint reaction force, generated a bending moment around the y-axis resulting in tensile stresses (0–20 MPa) in the ventral medial part and compressive stresses (0–20 MPa) in the dorsal lateral part of the acromion.

3.2. Scapular spine

The scapular spine is a thick bony structure providing elegant reinforcement to the scapula. Two of the major muscles, m. trapezius and m. deltoideus, are acting on the spine (Fig. 3). In the shoulder model there are six lines of forces of the m. trapezius and six lines of forces of the m. deltoideus, acting perpendicular to the spine, but in opposite directions. The scapular spine is

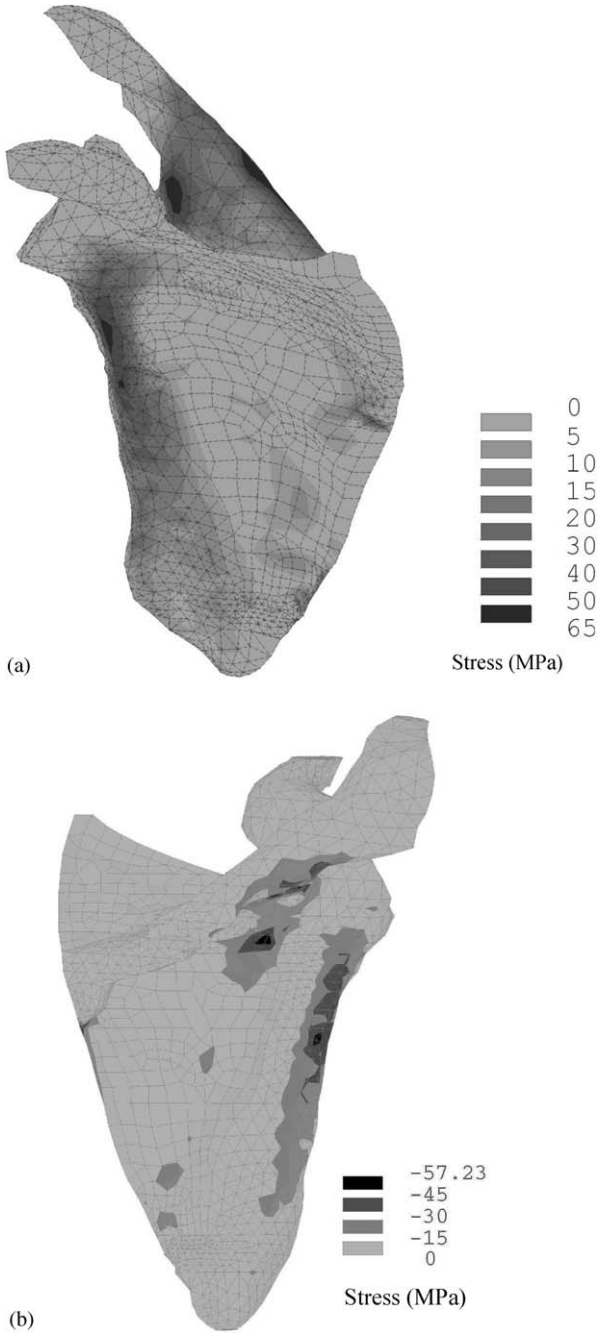

Fig. 4. Principal normal stress distribution (MPa) during 90° humeral abduction; (a) tensile (frontal-medial view); (b) compressive (dorsal view).

originating normally (branching out) from the vertical (scapular) plane of the fossa and is partly attached to the scapular neck (collum scapulae), which is located between the spine and the glenoid. Around 90° abduction, all parts of the m. trapezius become active to counteract the protracting force of m. serratus anterior. The m. deltoideus has the largest physiological cross-sectional area (PSCA) of the muscles of the shoulder mechanism, and exerts by far the largest moments around the GH-joint (Van der Helm, 1994a). During abduction, the muscle parts in the medial side are most active. The resulting force due to the action of m. trapezius and m. deltoideus lead to bending of the scapular spine. The bending effect resulted in high tensile (30–60 MPa) and compressive (−30 to −55 MPa) stresses in the cranial and caudal part of the spine, respectively (Fig. 4). It appeared that the infraspinous fossa represented a kind of tensional brace providing bending stress to the spine. The AC-joint reaction force also contributed to the bending effect of spine.

3.3. Glenoid

The GH-joint behaves as a spherical joint with a rotation centre fixed with respect to the scapula and has a large range of motions. During humeral elevation, muscle forces prevent the joint from dislocation by pressing the humeral head inside the glenoid. The position and insertions of the rotator cuff muscles, as a half circle around the humeral head, enables them to point the joint reaction force in almost any direction and acts as the main stabilising muscles of the GH-joint (Van der Helm, 1994a).

The stresses in this region largely depend on the position and direction of the GH-joint reaction force. At lower elevation angles, during abduction, the intersection point is more cranial than at higher elevation angles and is located at the anterior side of glenoid cavity (Van der Helm, 1991). The direction and magnitude of the GH-joint reaction force vectors in the global co-ordinate system are listed in Table 2. Evidently, the largest reaction forces were at 90-degree humeral abduction.

During 90° abduction, the point of application of GH-joint reaction force is located cranially, and at the anterior side of the glenoid cavity. The bulk of the GH-joint reaction force was carried by the glenoid and to a lesser degree by the lateral border (Fig. 4). The bending effect of the spine was partially transmitted to the glenoid, through the scapular neck. Stresses within the glenoid were largely compressive in nature. Higher stresses (20–50 MPa) were generated in the compact bone, whereas low stresses were (0–5 MPa) in the inner trabecular bone.

Table 2
Glenohumeral (GH) joint reaction forces during unloaded humeral elevation. Force components F_x, F_y, F_z corresponds to x, y and z directions, respectively, in the global co-ordinate system as shown in Figs. 1 and 2

Load case	Abduction angle (deg)	Force (N)		
		F_x	F_y	F_z
1	30	164.46	14.03	−16.14
2	60	323.74	−36.88	−3.68
3	90	383.71	−77.28	34.62
4	120	314.03	−137.96	45.56
5	150	137.74	−134.43	11.86
6	180	39.78	−72.51	−3.73

3.4. Lateral border

The lateral border is loaded by the reaction force at the thorax-AI connection and the m. serratus anterior inserting at AI on one side, and GH-joint reaction force on the other. The bending effect of scapular spine is partially transmitted to the lateral border, through the scapular neck. The combined effect results in severe bending of the lateral border, generating high tensile stresses (15–60 MPa) in the ventral side (Fig. 4a) and high compressive stresses (−15 to −55 MPa) in the dorsal side (Fig. 4b).

3.5. Connection of glenoid-spine-infraspinous fossa

The thick bony structures like the base of scapular spine, the glenoid and the lateral border are connected to the cranial part of the very thin, hard, laminated shell-like bone structure, the infraspinous fossa. A large bending moment is produced due to the combined action of: (1) the moment arising due to the action of m. trapezius and m. deltoideus, (2) the moment arising due to AC-joint reaction force, and (3) the moment arising due to the GH-joint reaction force. This resulted in generation of very high compressive stresses (45–58 MPa) at the junction of glenoid, spine and infraspinous fossa, which were the highest (compressive) in the whole scapula (Fig. 4b).

3.6. Medial border

In the present situation, the reactive forces of the thorax on the scapula were applied as concentrated forces, one at the thorax-AI connection and the other at the thorax-TS connection. In reality, however, this force is distributed along the medial border. During abduction the entire medial border is pressed to the thorax by the combined action of m. serratus anterior and upper part of m. rhomboideus (Van der Helm, 1994a). The thorax-AI reaction force, which is acting normal to the scapular plane, has a large moment arm about the local

x-axis through the scapular spine. The moment around this axis, arising due the pulling action of m. deltoideus on the spine also contributed to the bending effect of the medial border; generating tensile stresses at the ventral side and compressive stresses at the dorsal side. These stresses were low (1–10 MPa), except a few locations where it varied between 15–30 MPa (Fig. 4).

3.7. Trigonum spinae

The trigonum spinae (TS) is located at the medial border where the scapular spine is attached to the thin infraspinous and supraspinous fossa. During abduction the upper part of m. rhomboideus is counterbalancing the activity of upper part of m. serratus anterior, and together these muscles succeed to press the TS to the thorax (Van der Helm, 1994a). The lower part of m. serratus anterior, inserting at the AI, was able to produce large moments around the TS. The combined effect of two large forces, (1) m. serratus anterior, inserting at the AI, and (2) m. deltoideus, inserting at the lateral end of the spine, produced high bending moments, resulting in localised high stresses (45–60 MPa) in the TS (Fig. 4).

3.8. Angulus inferior

The Angulus Inferior is always pressed to the thorax by the lower part of m. serratus anterior. The reaction force at the thorax-AI connection (Fig. 3) increases with humeral abduction and is most active during 90° abduction, and reduces thereafter (Van der Helm, 1994a). The combined effect of m. serratus anterior and reaction force at the AI, generated localised stresses (15–30 MPa) as shown in Fig. 4a. Because of the large moment arm its effect was more redominant in the lateral border than at the AI.

3.9. Coracoid process

M. Biceps caput breve and m. coracobrachialis has a combined origin at the medial surface of the coracoid process (Fig. 3). The tendons of the caput breve and of the m. coracobrachialis are connected to a flat strong tendinous layer which continue to the coracoacromial ligament. Activity of the m. caput breve is reflecting the activity of m. coracobrachialis. The muscle is active after 60-degree abduction. The combined action of these muscles exerts a pulling force in the caudal (tip) part of the coracoid process, but it does not generate high stresses in the coracoid process.

3.10. Infraspinous and supraspinous fossa

Large fan shaped muscles (m. infraspinatus, m. supraspinatus, m. subscapularis) are attached to either sides of the infraspinous fossa and the supraspinous fossa. These muscles are mostly acting parallel to the fossa. The m. infraspinatus, attached to the dorsal side of infraspinous fossa, has a small moment arm around the sagittal axis till 60° abduction. At higher abduction angles, the moment arm becomes negative and the muscle is inactive. The force exerted by m. supraspinatus, attached to the dorsal side of supraspinous fossa, is small. The m. subscapularis, attached to the ventral side of infraspinous and supraspinous fossa, obtains a useful moment arm to counterbalance the external moment during abduction. Its activity is moderate during humeral abduction and exerts a maximum force of 60 N during 90° abduction. The combined effect of these three muscles generated a relatively low level of stress (tensile and compressive), varying between 0.05 and 15 MPa in most parts of infraspinous fossa, except a few locations adjacent to the medial border and the connection with spine-glenoid, where it varies between 15–24 MPa (Fig. 4). In contrast, the stresses generated in the supraspinous fossa are very low (0.05–5 MPa). During humeral abduction m. teres minor and m teres major are inactive (Van der Helm, 1994a).

3.11. Coracoacromial ligament

Due to the action of AC-joint reaction force and m. biceps caput breve, the nodes connected to form the ligament (beam) element were displaced away from one another (Fig. 2). Results indicated that the ligament is stretched, primarily in the $x-y$ plane.

4. Discussion

Most finite element studies on scapula deal with glenoid prostheses rather than the mechanics of scapula, as a whole (Orr et al., 1988; Friedman et al., 1992; Lacroix et al., 1997; Stone et al., 1999; Lacroix et al., 2000; Couteau et al., 2001). Using an experimentally validated FE model of the scapula (Gupta et al., in press), based on CT-scan data, the goal of this study was to understand the load transfer mechanism on the scapula due to muscles, ligaments, and joint reaction forces. A realistic estimate of the stress distribution was obtained, since the FE model and the static shoulder model of forces were based on the same cadaver (Van der Helm, 1994a,b).

The optimisation of the shape of the bone follows the action of muscles and tensional braces. The natural adaptation and optimisation of the shape of the bone with load is generally referred to as Wolff's law (1892). The scapula being no exception, its complicated shape must be related to the forces acting on it and to the induced stresses within it. Results indicated that the thick bony ridges are the 'pillars' of the scapula

structure. The scapular spine, the lateral border, the glenoid and the acromion supported the bulk of the load applied by major muscles, ligament and joint reaction forces. Similar idea was put forward by Anetzberger and Putz (1996). In the glenoid higher stresses (20–50 MPa) were generated in the compact bone layer covering the underlying cancellous bone, whereas stresses were low (0–5 MPa) in the underlying cancellous bone. Frich et al. (1997) presented average results obtained from 12 penetration tests at the three proximal levels of all ten specimens taken from the glenoid. The average strength of the glenoid at the proximal subchondral level was found to be 66.9 MPa. One millimetre underneath the subchondral plate, average strength decreased by 25% and at the 2 mm level strength decreased by 70% (Frich et al., 1997). It appears, therefore, that the stresses generated in the compact and the trabecular bones are within safe limits. The high stresses in the scapular spine were mainly due to the action of m. deltoideus, m. trapezius and AC-joint reaction forces. The stresses in the lateral border were also high; although the action of muscles attached in this region during humeral abduction is negligibly small. It is concluded that the transfer of high GH-joint reaction force and a part of the thorax-AI reaction force take place predominantly along the lateral border.

The function of each bony structure, which combines to form the complex 3D structure of the scapula, can not be precisely evaluated from this biomechanical study, since it is based on a single type of movement of the humerus, i.e. unloaded abduction. It appears that the stresses in the thick bony ridges were substantially higher as compared to the stresses in the infraspinous and supraspinous fossa. It appears, therefore, the fossa area acts more as attachment sites of large muscles. However, low stresses do not imply that the corresponding substructure is irrelevant for the overall stiffness of the scapula. Although this aspect was evident from this study, the shape of the scapula presumably is a compromise between many requirements. Stress analysis of the scapula using other loading conditions like, loaded abduction, loaded and unloaded anteflexion might lead to more precise answers to the question—why is the scapula structure so complicated and what are the function of its individual parts?

The boundary conditions used in this analysis are more appropriate than prescribing additional constraints to prevent rotation and translation. The reactive forces (constraints) computed by the FE model represent some type of physiologic forces that were left unspecified from the original force model (Table 1). These physiological constraints were useful to correct for residual moments that were produced due to slight change in the point of application of force. On the contrary, applying all the forces from the force model and prescribing additional constraints at these three points to avoid rigid body motion, unrealistically prevented relative motions of those constrained points, resulting in, additional reactive forces in the range of 7.5–11 N (arising due to residual moments) and therefore, localised stress. The forces acting near the constraints would have little effect on the stress fields elsewhere in the model. Hence, the constraints appear to be over-defined. It is therefore, more appropriate to use constraints that match a physiologic constraint, rather than just a fixation of nodes to prevent rigid body motion. This approach results in more realistic stress distributions in the scapula.

A few words must be said about the modelling artefacts. One of them is the high stress concentration in the TS, located at the medial border where the scapular spine is attached to the thin infraspinous fossa. This is primarily due to a combined effect of two large forces caused by the m. serratus anterior inserting at the AI, and the m. deltoideus inserting at the lateral end of spine. However, the additional (residual) reactive forces (of 8 N) generated at this location due to residual moments were not negligibly small, and therefore generated some stresses. The other major reason could be due to the wedge shaped structure of bone in that location, which gradually tapers to an extremely thin bone (Fig. 4). Probably, at this particular area the present model generates rather inadequate results for stresses and strains. Another modelling artefact in the medial border may be caused due to the application of concentrated forces, due to thorax-AI and thorax-TS joint reactions and m. serratus anterior. But in reality, these forces are distributed along the entire length of the medial border. In general, the muscle, ligament and joint reaction forces were applied as concentrated loads in the FE model. In reality, however, the forces should be distributed on the surface of those elements that are located in the areas of insertion, which are yet to be investigated.

The functional aspect of the coracoacromial ligament was unknown, qualitatively and quantitatively. Since nothing is known about its stress–strain characteristics and its length, only a qualitative prediction was obtained from this study. It should however be noted the effect of this ligamentous structure on the complete functional system, i.e. the scapula, and in particular, the glenoid, remains to be investigated. It appears that the ligament is stretched, primarily in the frontal ($x-y$) plane, and presumably will be under tension during humeral abduction.

5. Conclusions

Based on an experimentally validated realistic 3D FE model of the scapula, using CT-scan data and the static shoulder model of forces, the effect of load transfer

mechanism in the form of stress distribution can be studied. The following are the specific conclusions of this study:

(1) The thick bony structures of the scapula were subject to high stresses as compared to low stresses in the fossa areas, which indicated that the function of fossa areas was to act as attachment sites of large muscles rather than sharing of load.
(2) High stresses, tensile and compressive are observed on cranial and caudal side of scapular spine, respectively, indicating bending of the spine.
(3) The acromion is subject to bending due to the action of pulling force by m. deltoideus and AC-joint reaction force resulting in tensile and compressive stresses in the ventral-medial part and dorsal–lateral part.
(4) The most important force of the scapula, the GH-joint reaction force, and a part of the thorax-AI joint reaction force were predominantly transferred along the lateral border resulting in severe bending of the lateral border.
(5) High compressive stresses were evoked in the glenoid; but these stresses were below the strength of glenoid compact and trabecular bone.
(6) High compressive stresses were generated at the glenoid-scapular spine-infraspinous fossa junction.

References

Anetzberger, H., Putz, R., 1996. The scapula: principles of construction and stress. Acta Anatomica 156 (1), 70–80.

Couteau, B., Manset, P., Estivalezes, E., Darmana, R., Mansat, M., Egan, J., 2001. Finite element analysis of the mechanical behavior of a scapula implanted with a glenoid prosthesis. Clinical Biomechanics 16, 566–575.

Frich, L.H., Jensen, N.C., Odgaard, A., Pedersen, C.M., Søjbjerg, J.O., Dalstra, M., 1997. Bone strength and material properties of the glenoid. Journal of Shoulder and Elbow Surgery 6, 97–104.

Friedman, J.R., LaBerge, M., Dooley, R.L., O'Hara, A.L., 1992. Finite element modelling of the glenoid component: effect of design parameters on stress distribution. Journal of Shoulder and Elbow Surgery 1, 261–270.

Gupta, S., Van der Helm, F.C.T., Sterk, J.C., Van Keulen, F., Kaptein, B.L. in press. Development and experimental validation of a three-dimensional finite element model of the human scapula. Journal of Engineering in Medicine (Proc. Inst. Mech. Engrs. Part H).

Lacroix, D., Prendergast, P.J., Murray, R., McAlinden, S., D'Arcy, E., 1997. The use of quantitative computed tomography to generate a finite element model of the scapula. In: Monaghan J., Lyons, C.G. (Eds.), Proceeding of the 14th Conference Irish Manufacturing Committee, pp. 257–262.

Lacroix, D., Murphy, L.A., Prendergast, P.J., 2000. Three-dimensional finite element analysis of glenoid replacement prosthesis; a comparison of keeled and pegged anchorage systems. Journal of Biomechanical Engineering 122, 430–436.

Levy, O., Copeland, S.A., 2001. Regeneration of the coracoacromial ligament after acromioplasty and arthroscopic subacromial decompression. Journal of Shoulder and Elbow Surgery 10 (4), 317–320.

Orr, T.E., Carter, D.R., Schurman, D.J., 1988. Stress analyses of glenoid component designs. Clinical Orthopaedics and Related Research 232, 217–224.

Stone, K.D., Grabowski, J.J., Cofield, R.H., Morrey, B.F., An, K.N., 1999. Stress analysis of glenoid components in total shoulder arthroplasty. Journal of Shoulder and Elbow Surgery. 8 (2), 151–158.

Van der Helm, F.C.T., 1991. The shoulder mechanism, a dynamic approach. Ph.D. Thesis, Delft University of Technology, Delft, The Netherlands.

Van der Helm, F.C.T., Veenbaas, R., 1991. Modelling the mechanical effect of muscles with large attachment sites: application to the shoulder mechanism. Journal of Biomechanics 24 (12), 1151–1163.

Van der Helm, F.C.T., 1994a. Analysis of the kinematic and dynamic behaviour of the shoulder mechanism. Journal of Biomechanics 27, 527–550.

Van der Helm, F.C.T., 1994b. A finite element musculoskeletal model of the shoulder mechanism. Journal of Biomechanics 27, 551–569.

Wolff, J., 1892. Das Gesetz der Transformation der Knochen. Berlin, Hirchwild (Translated as The Law of Bone Remodelling). Springer, Berlin, 1986.